# Supporting Information

## A Facile Silicon Doping Strategy Constructing "M-O-Si" Bonds in ZnCo-LDH for Efficient Neutral Nitrate Reduction to Ammonia and Zn-$NO_3^-$ Battery

Kunxuan Zhao[a,#], Pei Chen[a,#], Yulan Shi[a], Zhen Yang[a], Xia Zhou[a], Jinfeng Yang[a,*], Xiaodong Yang[b,*], Feng Yu[a,*]

[a] Key Laboratory of Silicon Chemical New Materials, School of Chemistry and Chemical Engineering, Shihezi University, Shihezi 832003, P.R. China
[b] College of Sciences, Shihezi University, Shihezi 832003, China

*Corresponding authors.
E-mail addresses: yangjinfeng@shzu.edu.cn (J. Yang), yangxiaodong1209@hotmail.com (X. Yang) yufeng05@mail.ipc.ac.cn (F. Yu).

[#] These authors contributed equally to this work.

In this file includes the following information:

- Experimental
- Figures S1-S26
- Tables S1-S5
- References

# 1. Experimental

## 1.1 Characterizations

X-ray diffraction spectra (XRD) were obtained by a Bruker D8 Advance X-ray diffractometer with a Cu Kα radiation source (wavelength λ = 1.541 nm). The scanning range was set to 5-90° with a scanning rate of 5°/min. Scanning electron micrographs and transmission electron micrographs were obtained with a Hitachi S4800 scanning electron microscope and a FEI Tecnai G2 F20 transmission electron microscope equipped with an energy dispersive X-ray spectrometer. x-ray photoelectron spectroscopy (XPS) was obtained by Thermo Fisher Scientific Thermo ESCALAB 250XI instrument was obtained. Fourier transform infrared spectra (FTIR) were obtained using a Bruker Vertex 70. Raman spectra were obtained using a Renishaw invia type instrument (UK). Online differential electrochemical mass spectrometry (DEMS) measurements was performed utilizing the QAS 100 instrument manufactured by LingLu Instruments (China).

## 1.2 Electrochemical measurements

All electrochemical measurements for electrochemical $NO_3^-$RR were carried out in a standard three-electrode system, using a CHI 660E electrochemical workstation for data collection. The standard three-electrode system was a reference electrode (Hg/HgO electrode), a counter electrode (Pt sheet), and a working electrode (Si-ZnCo-LDH/Cu and ZnCo-LDH/Cu). The H-type electrolytic cell separated the cathode and anode chambers with a Nafion 117 membrane, and the two chambers were each filled with 50 mL of 0.5 M $Na_2SO_4$ (0.1 M $NO_3^-$) electrolyte. Linear scanning voltammetry (LSV) tests were performed in the potential range of

0.1 V ~ −1.5 V vs. RHE at a scan rate of 10 mV $s^{-1}$ until the polarization curve was stable. Constant potential (i-t) measurements were performed by applying a series of potentials for 1 h at room temperature, the electrolyte was replaced with a new one for the next test. Electrochemical impedance spectroscopy (EIS) measurements were performed in a solution of 0.5 M $Na_2SO_4$, where the frequency range was 1-100 kHz, the AC amplitude was 5 mV, and the bias potential was −1.5 V vs. RHE. All potentials were referenced to the RHE ($E_{RHE}$ = $E_{Hg/HgO}$ + 0.0591 × pH + 0.098), and the current densities were normalized to the currents per square centimeter of the of the geometric area.

***Faradaic efficiency and yield of $NH_3$:***

The yield (mg $h^{-1}$ $cm^{-2}$) of $NH_3$ was computed by the subsequent equation:

$$\text{Yield } (NH_3) = (C_{NH3} \times V) / (t \times A) \times 10^{-3} \quad (1)$$

Where $C_{NH3}$ is the concentration of $NH_3$ (μg/mL) in the electrolyte, V is the volume of the electrolyte (mL), t is the electrolysis time (1 h), A is the geometric area of the electrode (1 $cm^2$).

The faradaic efficiency (FE, %) of $NH_3$ production was ascertained by the following equation:

$$FE\ (NH_3) = (8 \times F \times C_{NH3} \times V \times 10^{-16}) / (17 \times Q) \times 100\% \quad (2)$$

Where F is Faraday constant (96485 C $mol^{-1}$), Q is the charge consumed for electrolysis process (C).

***Selectivity of $NH_3$ and $NO_2^-$:***

The selectivity (S, %) of $NH_3$ was computed by the subsequent equation:

$$S\ (NH_3) = C_{NH3} / (C_{(NO3-)0} - C_{(NO3-)t}) \times 100\% \quad (3)$$

The selectivity (S, %) of $NO_2^-$ was computed by the subsequent equation:

$$S\ (NO_2^-) = C_{NO2-} / (C_{(NO3-)0} - C_{(NO3-)t}) \times 100\% \quad (4)$$

***Removal rate of $NO_3^-$:***

The removal rate (R, %) of $NO_3^-$ was computed by the subsequent equation:

$$R\ (NO_3^-) = (C_{(NO3-)0} - C_{(NO3-)t}) / C_{(NO3-)0} \times 100\% \quad (5)$$

Where $C_{(NO3-)0}$ is the initial concentration of $NO_3^-$ (μg/mL) in the electrolyte, $C_{(NO3-)t}$ is the concentration of $NO_3^-$ (μg/mL) in the electrolyte after electrolysis, $C_{NO2-}$ is the concentration of $NO_2^-$ (μg/mL) in the electrolyte.

***Determination of ammonia content:***

The determination of $NH_3$ is accomplished by employing the indophenol blue colorimetric method using UV-vis spectroscopy. A certain quantity of electrolyte is withdrawn from the electrolyzer and diluted 100-fold to fall within the detection range. Incorporate 2 mL of sodium salicylate solution (5 wt% salicylic acids, 5 wt% sodium citrate dihydrate in 1 M NaOH), 1 mL of NaClO solution (0.05 M), and 0.2 mL of sodium nitroprusside solution into 2 mL of the sample solution (5 wt%). After 1 h incubation, UV-vis spectra were recorded (500-800 nm) The absorption peak at 655 nm originated from the formation of indophenol blue. The concentration-absorbance curve was calibrated by employing a series of standard ammonium chloride solutions (0.00, 0.25, 0.50, 1.00, 1.50, 2.00, 2.50, 6.00, 10.00 μg/mL).

***Determination of nitrate content:***

Nitrate ($NO_3^-$) concentrations were spectrophotometrically quantified by adding 0.1 mL of 1 M HCl and 0.01 mL of 0.8 wt% sulfamic acid solution to the diluted sample (5 mL).

Absorbance values were recorded at 220 nm and 275 nm. The final absorbance was calculated as $A = A_{220nm} - 2A_{275nm}$, correcting for potential interferences. A series of standard potassium nitrate solutions were used to obtain the concentration–absorbance curve by the same processes.

***Determination of nitrite content:***

Nitrite ($NO_2^-$) concentrations were spectrophotometrically quantified using a colorimetric assay. A color reagent was prepared by dissolving 0.02 g N-(1-naphthyl) ethylenediamine dihydrochloride and 0.4 g p-aminobenzenesulfonamide in 5 mL deionized water, adding 1 mL phosphoric acid ($\rho = 1.685$ g $mL^{-1}$), and mixing thoroughly. For analysis, electrolyte samples from the electrolytic cell were diluted to within the detection range. Then, 5 mL of the diluted sample were mixed with 0.1 mL of color reagent. After 20 minutes at room temperature, the absorption spectrum was measured using a UV-vis spectrophotometer, and the absorbance was recorded at 540 nm. A series of standard sodium nitrite solution were used to obtain the concentration-absorbance curve by the same procedure.

***Electrochemical in-situ ATR-FTIR reflection spectroscopy:***

*In-situ* ATR-FTIR spectra (1000~2000 $cm^{-1}$, 4 $cm^{-1}$ resolution) were recorded on a Bruker INVENIO S spectrometer using a custom three-electrode reactor (Beijing Science Star Technology Co. Ltd, China). In the ATR-FTIR measurements, a reference spectrum ($R_{Ref}$) was collected at the open circuit potential, after which the potential was stepped to the target value ($E_S$) to acquire the working spectrum ($R_S$). The resulting spectra are presented as the relative change in reflectance: $\Delta R/R = (R(E_S) - R(E_R))/R(E_R)$. The $R(E_S)$ and $R(E_R)$ refer to the single-beam spectra detected at sample potential and reference potential, respectively. Downward-oriented bands indicate the formation of $NO_3^-$-related intermediates at $E_S$, while upward-

oriented bands correspond to the consumption of $NO_3^-$. The electrochemical in-situ ATR-FTIR spectroscopy was collected from −0.5 V to −1.7 V every 200 mV in 0.5 M $Na_2SO_4$ +0.1 M $KNO_3$.

***Electrochemical in-situ Raman spectroscopy:***

*In-situ* Raman spectra were recorded on a Renishaw Qontor Raman spectrometer (Invia) with an excitation wavelength of 514 nm and a 50 x objective (100~3200 $cm^{-1}$, 2 $cm^{-1}$ resolution) using a custom three-electrode reactor (Beijing Science Star Technology Co. Ltd, China). The test potentials were the same as those in the electrochemical *in-situ* ATR-FTIR tests.

***Differential electrochemical mass spectrometry (DEMS) measurements:***

DEMS was performed utilizing the QAS 100 instrument manufactured by LingLu Instruments (China). The electrolyte solution is 0.5 M $Na_2SO_4$ with 0.1 M $KNO_3$. The working electrode is Si-ZnCo-LDH/Cu and ZnCo-LDH/Cu, the reference electrode is a Hg/HgO electrode, and the counter electrode is a Pt wire. The linear scanning voltammetry (LSV) test was performed in the voltage range of 0 V ~ −1.3 V vs. RHE with a scan rate of 10 mV $s^{-1}$ until the corresponding mass signal appeared after the baseline was stabilised. After the electrochemical test was completed, the next cycle was initiated when the mass signal returned to the baseline, and the experiment was terminated after completing four cycles.

**1.3 Density functional theory (DFT) calculations**

The DFT calculations were performed using the Vienna Ab initio Simulation Package (VASP). The interaction between valence and core electrons was handled via the Projected Augmented Wave (PAW) method. Plane-wave propagation with a cutoff energy of 500 eV

ensured sufficient computational accuracy. Interfacial interactions were described using the Perdew-Burke-Ernzerhof (PBE) functional combined with van der Waals corrections (DFT-D3). K-point sampling in the first Brillouin zone was implemented using a Γ-centered Monkhorst-Pack scheme, with an 8×8×1 grid for the ZnCo-LDH/Cu heterostructure. A vacuum layer of approximately 20 Å was introduced along the Z-direction to prevent interactions arising from periodic adjacent interfaces. During geometric optimization, the convergence criterion for energy per atom was set to $10^{-7}$ eV, while the force convergence criterion was set to $10^{-5}$ eV/Å. The ZnCo-LDH/Cu catalyst model consists of 90 atoms, including 8 Zn atoms, 6 Cu atoms and 4 Co atoms; the Si-ZnCo-LDH/Cu catalyst model consists of 90 atoms, including 8 Zn atoms, 6 Cu atoms, 4 Co atoms and 3 Si atoms. Based on the computational hydrogen electrode model, the Gibbs free energy (ΔG) for each elementary step can be expressed as follows:

$$\Delta G = \Delta E + \Delta E_{ZPE} - T\Delta S + \Delta pH$$

Where ΔE represents the energy from DFT calculations, and $\Delta E_{ZPE}$ and ΔS denote the corrections for zero-point energy and entropy, respectively. T is temperature (298.15 K). ΔpH is the effect of pH value.

The process of electrochemical reduction of nitrates to ammonia involves nine protons and eight electrons. The entire reaction can be summarized as follows:

$$NO_3^- + 9\,H^+ + 8e^- \rightarrow NH_3 + 3H_2O$$

which include 9 reactions as follows (* represents the adsorption site):

$$* + NO_3^- \rightarrow {}^*NO_3 + e^- \qquad (1)$$

$$^{*}NO_3 + 2H^+ + 2e^- \rightarrow {}^{*}NO_2 + H_2O\,^{*} \quad (2)$$

$$^{*}NO_2 + 2H^+ + 2e^- \rightarrow {}^{*}NO + H_2O \quad (3)$$

$$^{*}NO + H^+ + e^- \rightarrow {}^{*}NOH \quad (4)$$

$$^{*}NOH + H^+ + e^- \rightarrow {}^{*}NHOH \quad (5)$$

$$^{*}NHOH + H^+ + e^- \rightarrow {}^{*}NH_2OH \quad (6)$$

$$^{*}NH_2OH + H^+ + e^- \rightarrow {}^{*}NH_2 + H_2O \quad (7)$$

$$^{*}NH_2 + H^+ + e^- \rightarrow {}^{*}NH_3 \quad (8)$$

$$^{*}NH_3 \rightarrow {}^{*} + NH_3 \quad (9)$$

## 2. Supplementary Figures

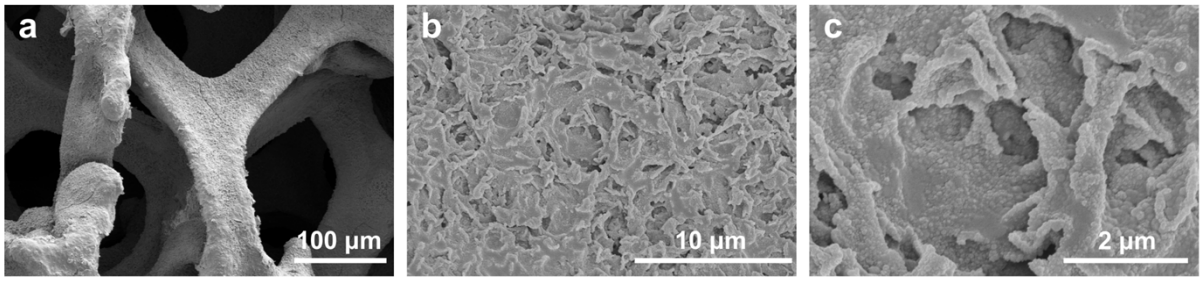


**Fig. S1.** SEM image of Si-ZnCo-LDH/Cu with different molar ratios (a) 100 µm, (b) 10 µm and (c) 2 µm.

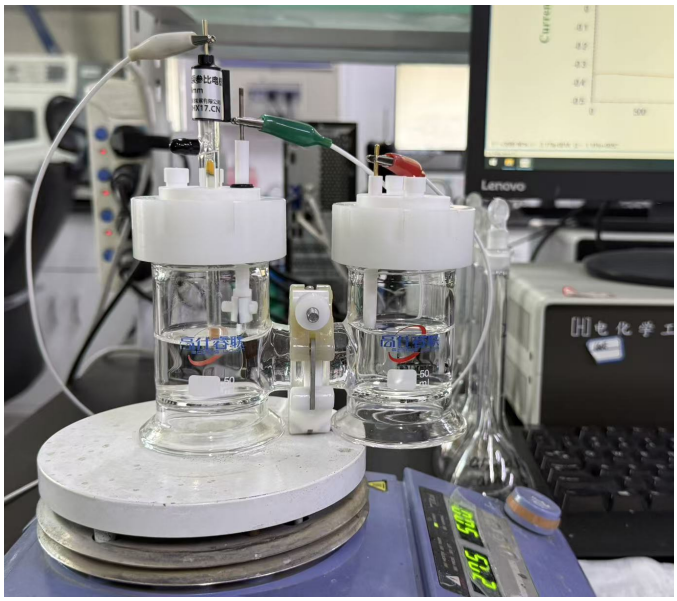


**Fig. S2.** The photograph of electrochemical setup for $NO_3^-$RR test.

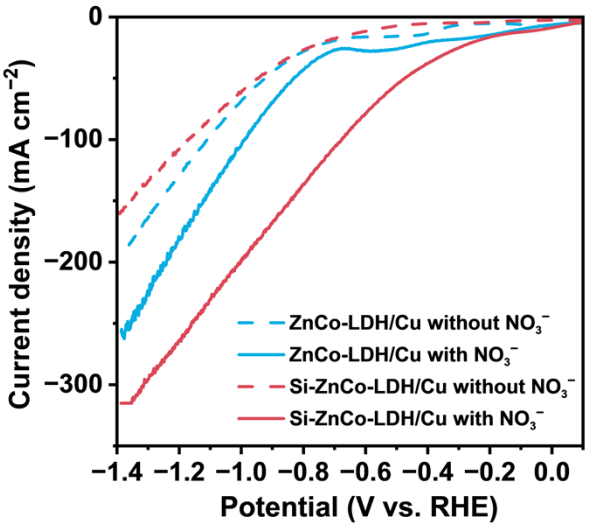


**Fig. S3.** LSV of ZnCo-LDH/Cu and Si-ZnCo-LDH/Cu in 0.5M $Na_2SO_4$ electrolyte when $NO_3^-$ is absent (dotted line) and $NO_3^-$ is present (solid line).

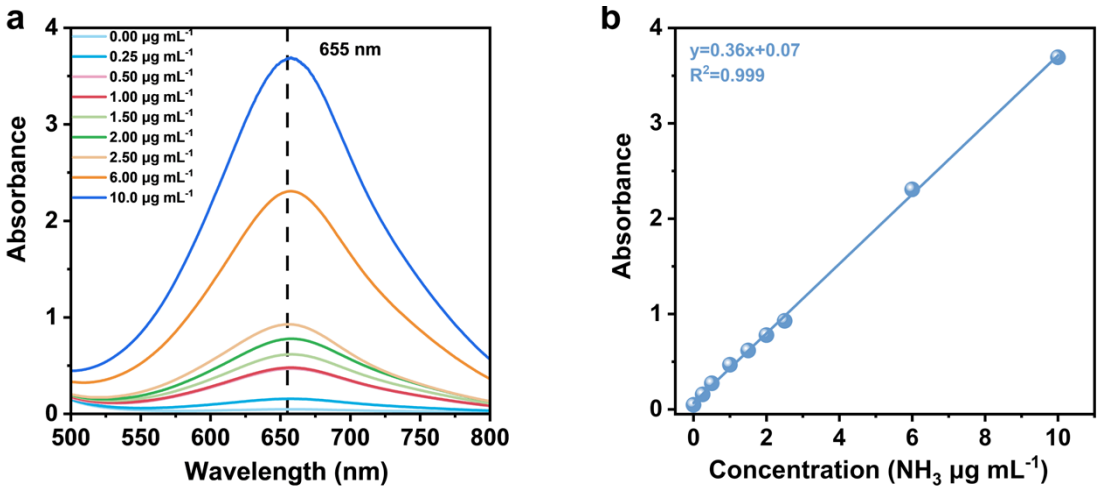


**Fig. S4.** UV-visible calibration curves for $NH_3$ were established by using a standard solution of ammonium chloride at a known concentration. (a) UV-vis curves of indophenol assays with $NH_3$ and (b) calibration curves of $NH_3$ concentrations at the wavelength of 655 nm.

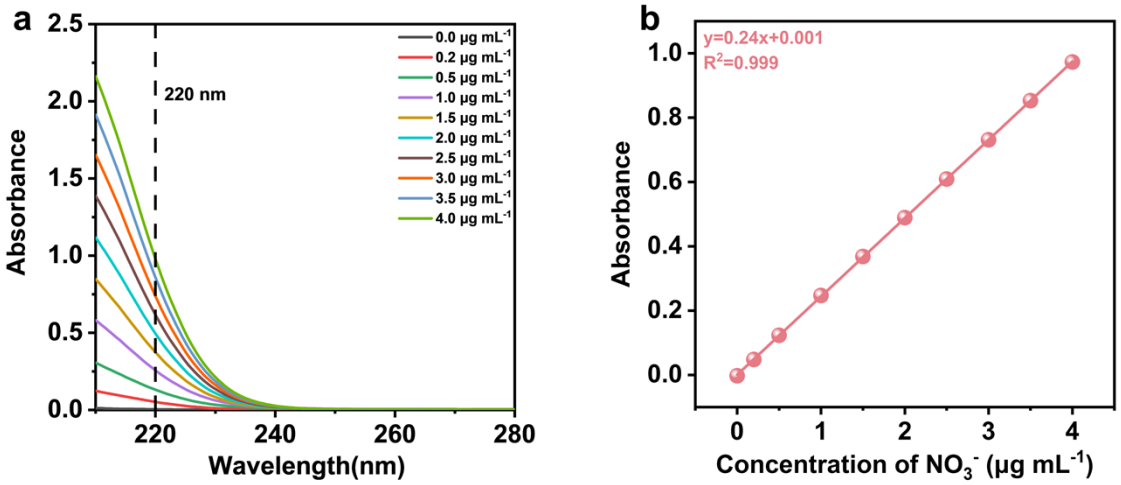


**Fig. S5.** UV-visible calibration curves for $NO_3^-$ were established by using a standard solution of potassium nitrate at a known concentration. (a) UV-vis curves of indophenol assays with $NO_3^-$ and (b) calibration curves of $NO_3^-$ concentrations at the wavelength of 220 nm.

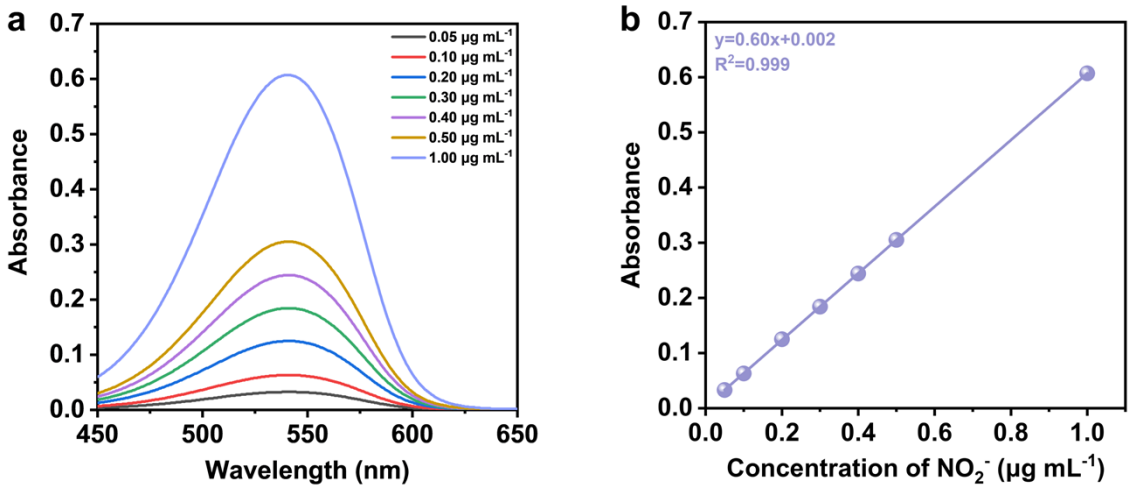


**Fig. S6.** UV-visible calibration curves for $NO_2^-$ were established by using a standard solution of sodium nitrite at a known concentration. (a) UV-vis curves of indophenol assays with $NO_2^-$ and (b) calibration curves of $NO_2^-$ concentrations.

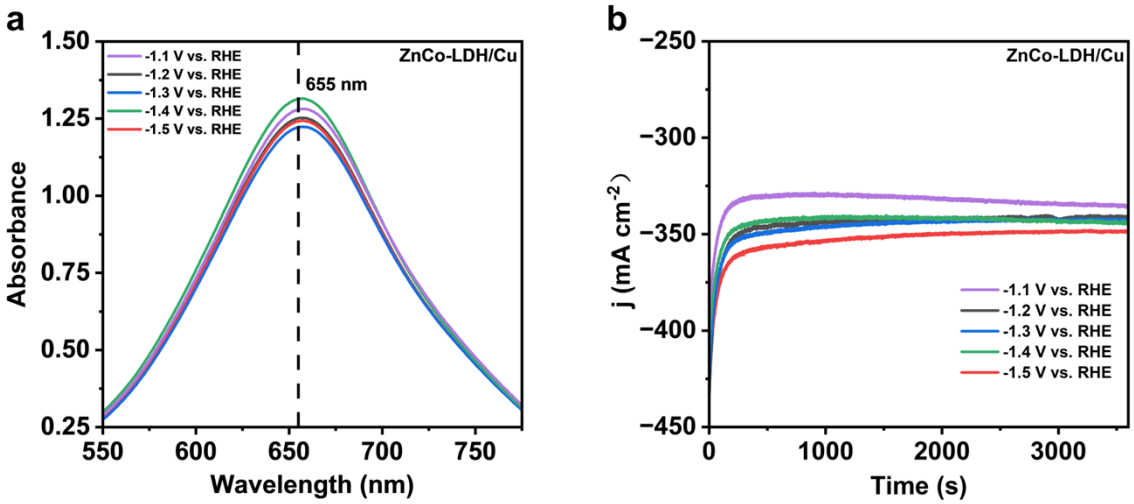


**Fig. S7.** ZnCo-LDH/Cu of (a) UV-vis absorption spectra of the electrolytes stained after electrolysis for 1 hours at different potentials. (b) Current density curves vary with time.

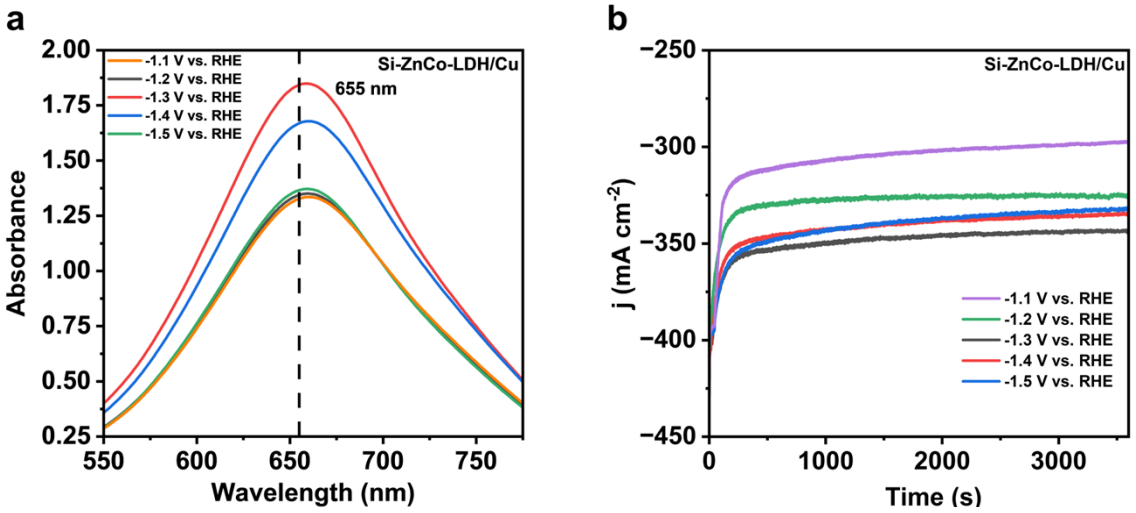


**Fig. S8.** Si-ZnCo-LDH/Cu of (a) UV-vis absorption spectra of the electrolytes stained after electrolysis for 1 hours at different potentials. (b) Current density curves vary with time.

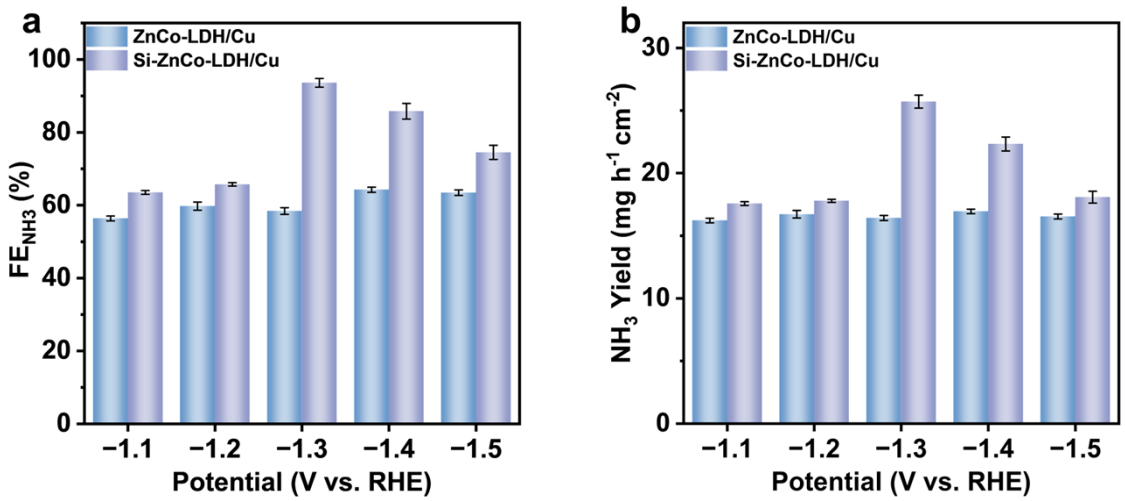


**Fig. S9.** (a) $FE_{NH3}$ and (b) ammonia yields corresponding to ZnCo-LDH/Cu and Si-ZnCo-LDH/Cu at different applied potentials.

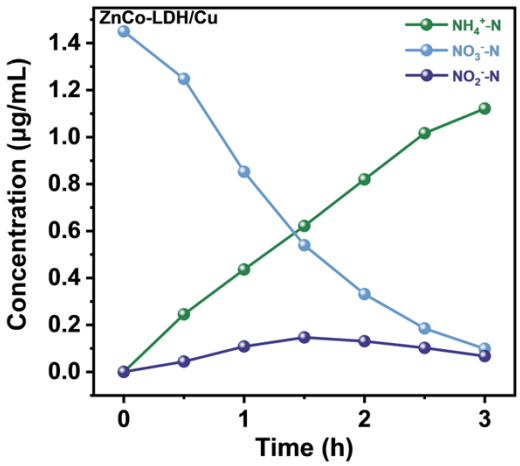


**Fig. S10.** ZnCo-LDH/Cu of the concentrations of $NH_4^+$-N, $NO_3^-$-N and $NO_2^-$-N in the electrolyte varied with time at −1.3V vs. RHE.

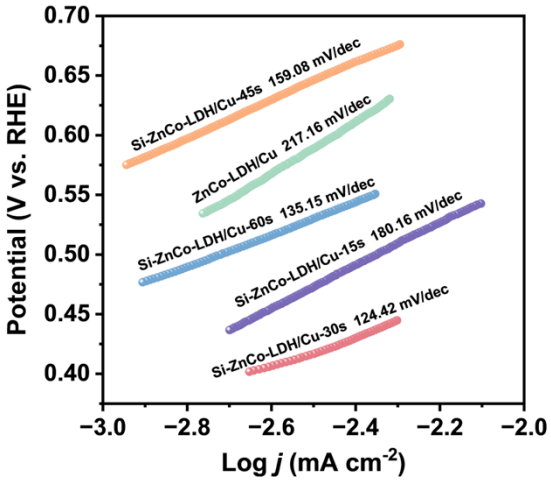


**Fig. S11.** The Tafel slope of different samples.

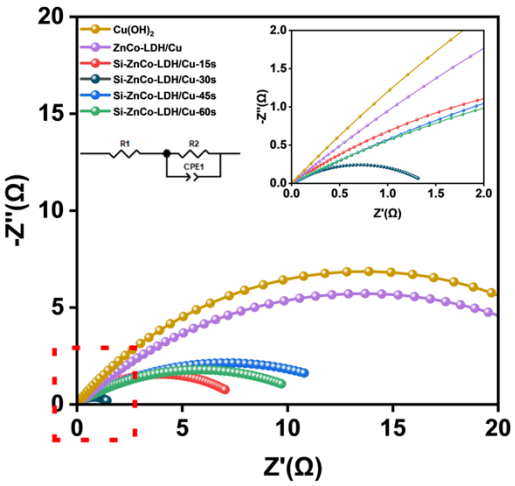


**Fig. S12.** EIS spectra of different samples.

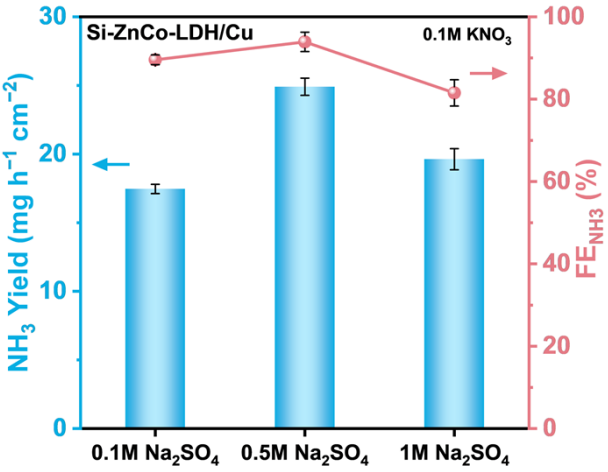


**Fig. S13.** Yield rate and FE of $NO_3^-$RR to ammonia on Si-ZnCo-LDH/Cu in 0.1 M $KNO_3$ and 0.1 M, 0.5 M and 1 M$Na_2SO_4$ electrolyte.

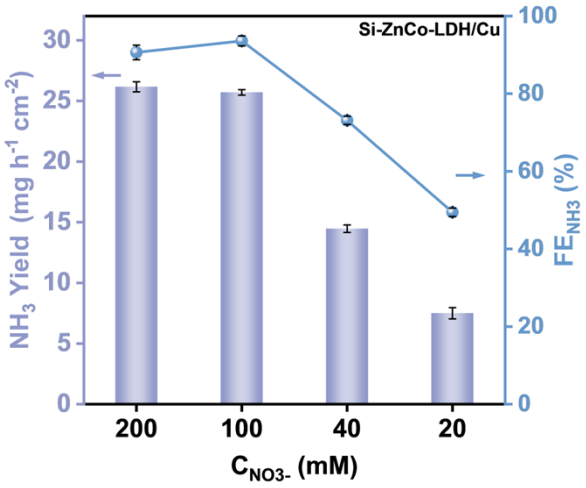


**Fig. S14.** Si-ZnCo-LDH/Cu of Yield rate and $FE_{NH3}$ of $NO_3^-$RR to ammonia on Si-ZnCo-LDH/Cu in 0.5 M $Na_2SO_4$ electrolyte with 20 mM, 40 mM, 100 mM and 200 mM $NO_3^-$.

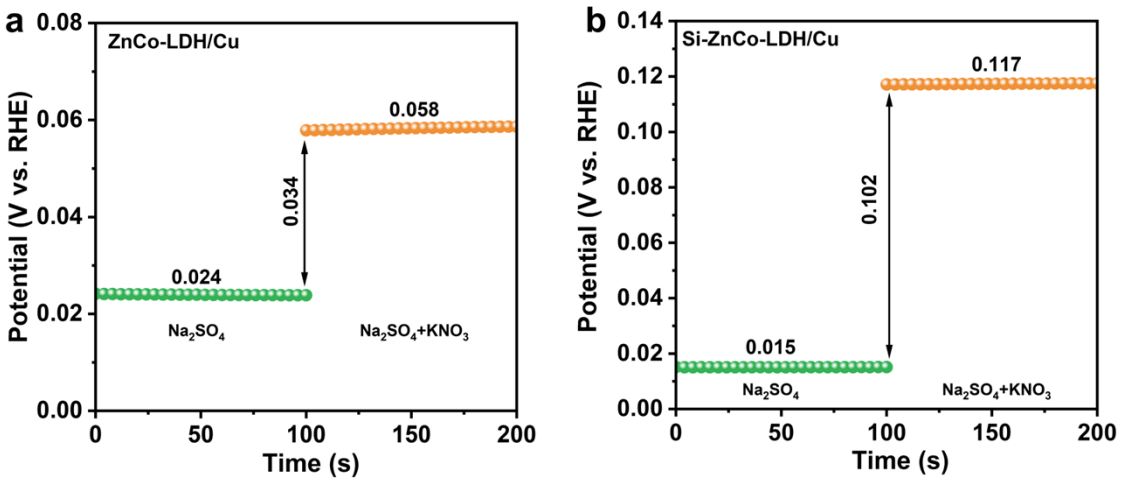


**Fig. S15.** Open circuit potentials of (a) ZnCo-LDH/Cu and (b) Si-ZnCo-LDH/Cu in $Na_2SO_4$ with and without $KNO_3$.

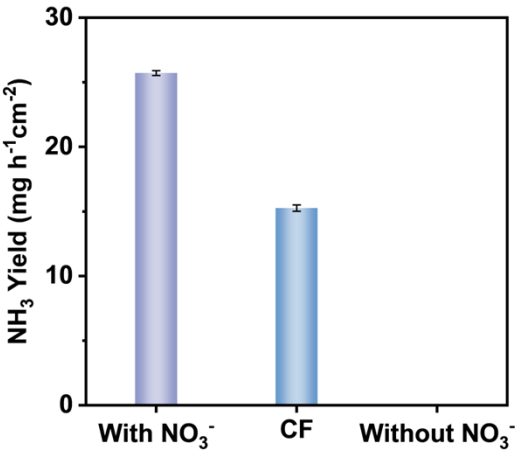


**Fig. S16.** The Yield rate of ammonia in 0.5 M $Na_2SO_4$ electrolyte with $NO_3^-$, CF, and without $NO_3^-$.

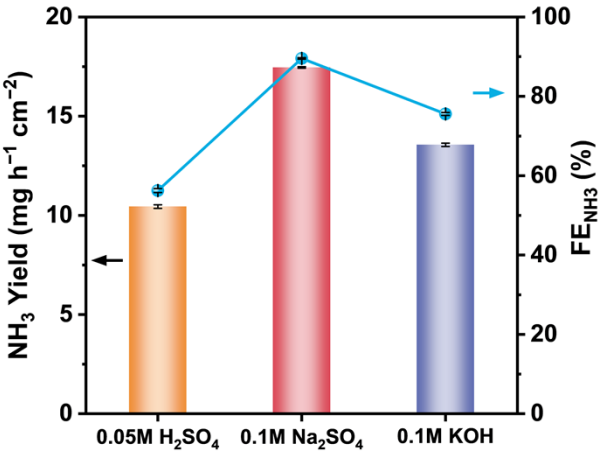


**Fig. S17.** Yield rate and FE of $NO_3^-$RR to ammonia on Si-ZnCo-LDH/Cu in 0.05 M $H_2SO_4$, 0.1 M $Na_2SO_4$ and 0.1 M KOH electrolyte.

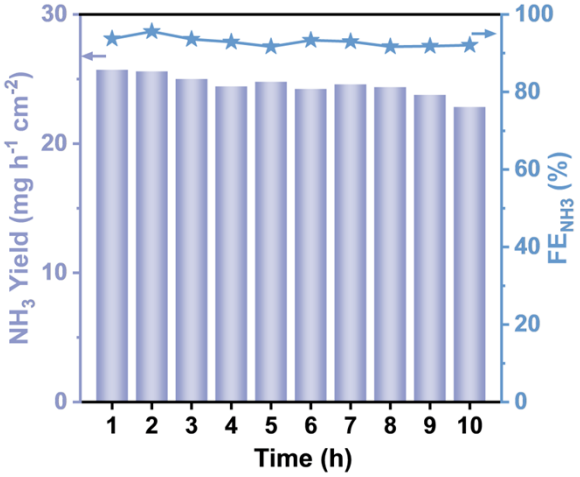


**Fig. S18.** Stability results after 10 cycles of Si-ZnCo-LDH/Cu.

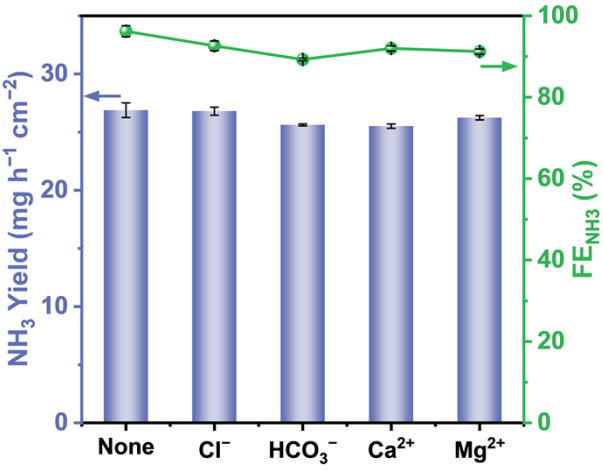


**Fig. S19.** The influence of cationic and anionic impurities on $NO_3^-$RR.

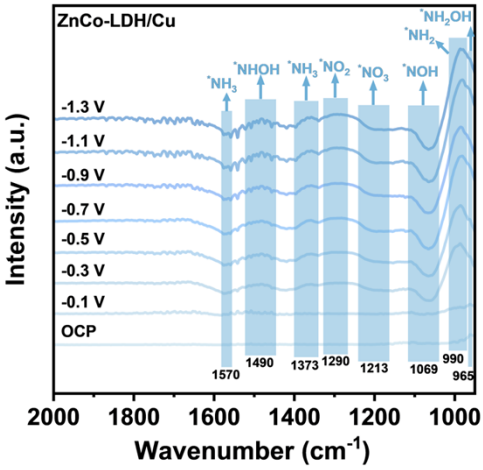


**Fig. S20.** Electrochemical *in-situ* ATR-FTIR spectra of the ZnCo-LDH/Cu.

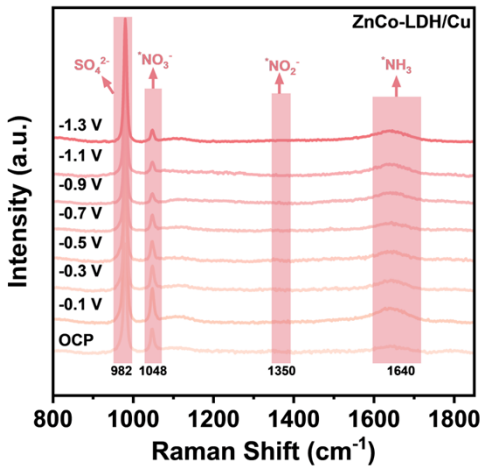


**Fig. S21.** Electrochemical *in-situ* Raman spectra of the ZnCo-LDH/Cu.

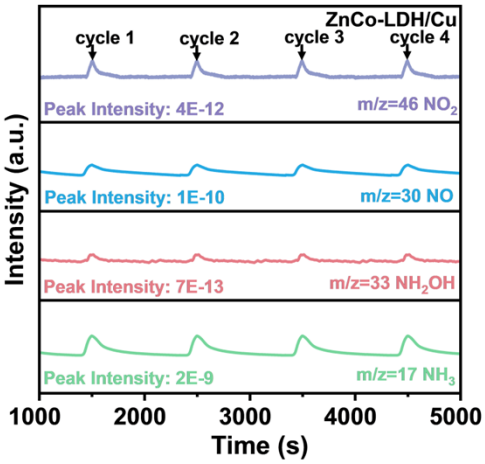


**Fig. S22.** Electrochemical DEMS measurements of $NO_3^-$RR of the ZnCo-LDH/Cu.

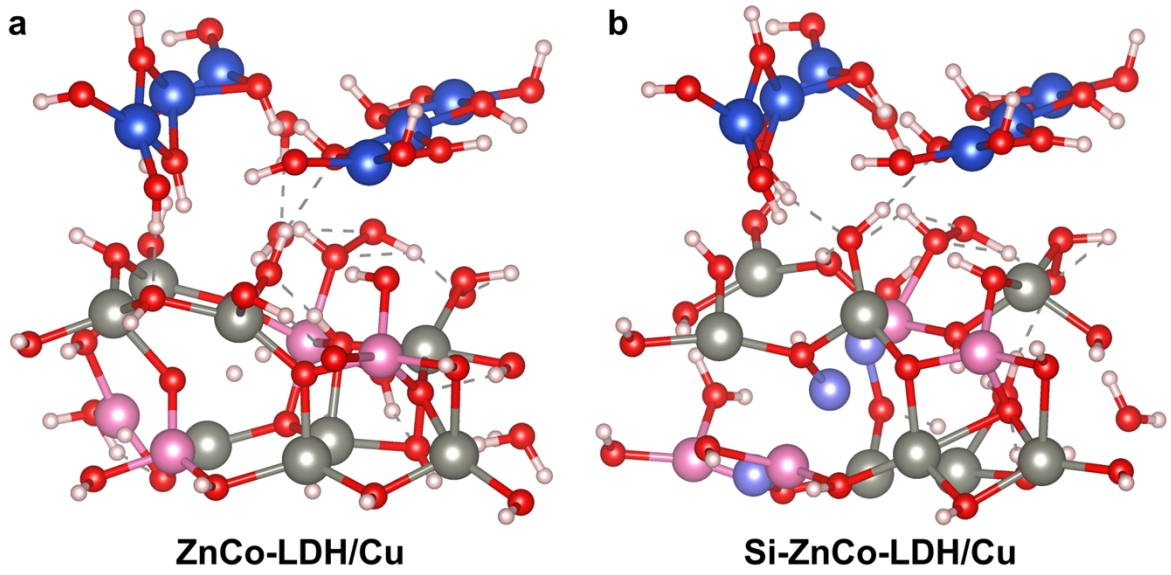


**Fig. S23.** Structural diagram of the catalyst substrate.

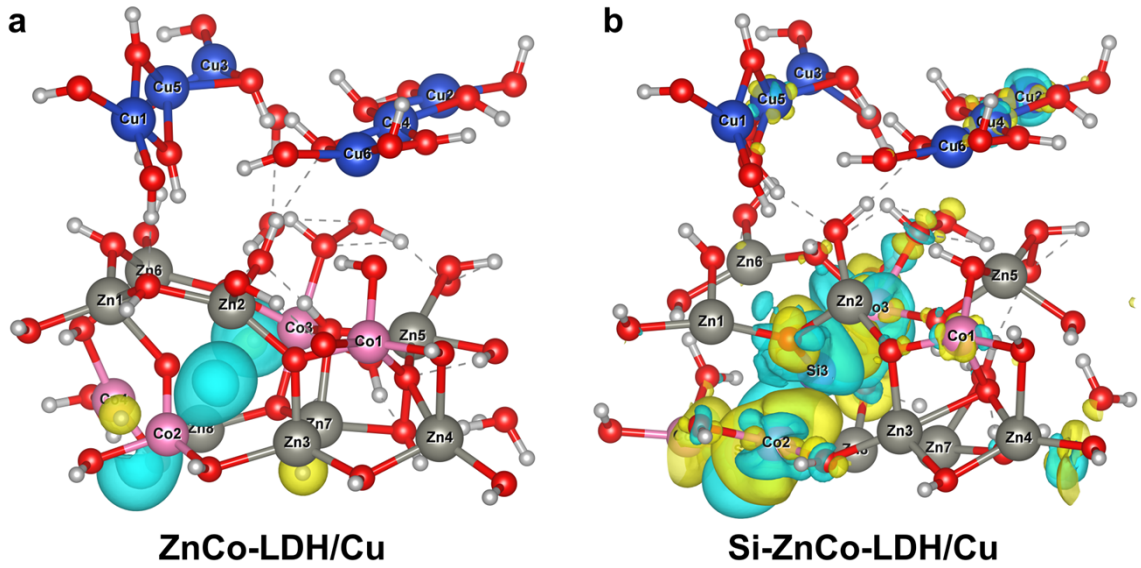


**Fig. S24.** Charge density difference of the interface the catalyst, where yellow color represents charge accumulation and blue color represents charge depletion.

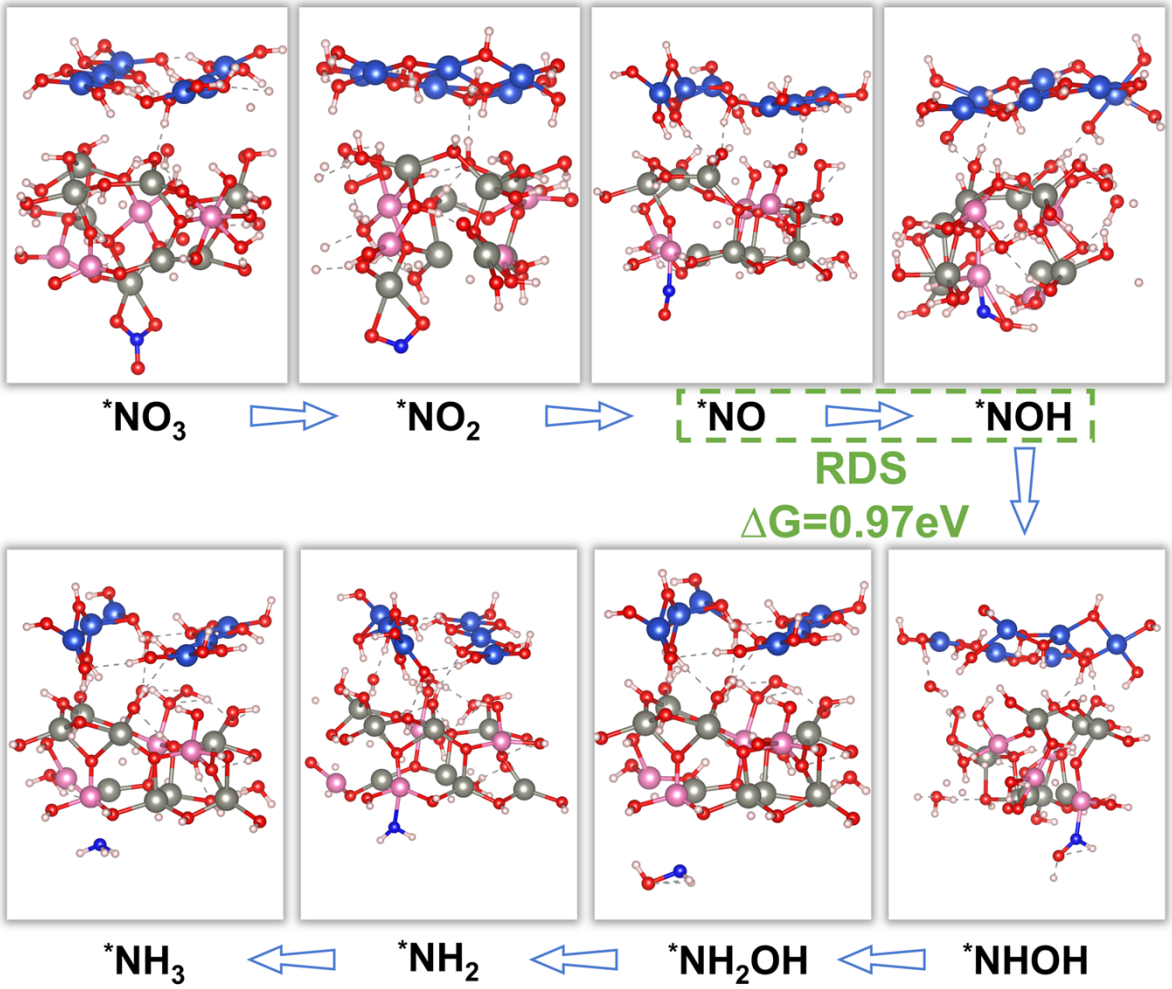


**Fig. S25.** Model diagram of the adsorption of intermediates by ZnCo-LDH/Cu catalyst in the $NO_3^-$RR process.

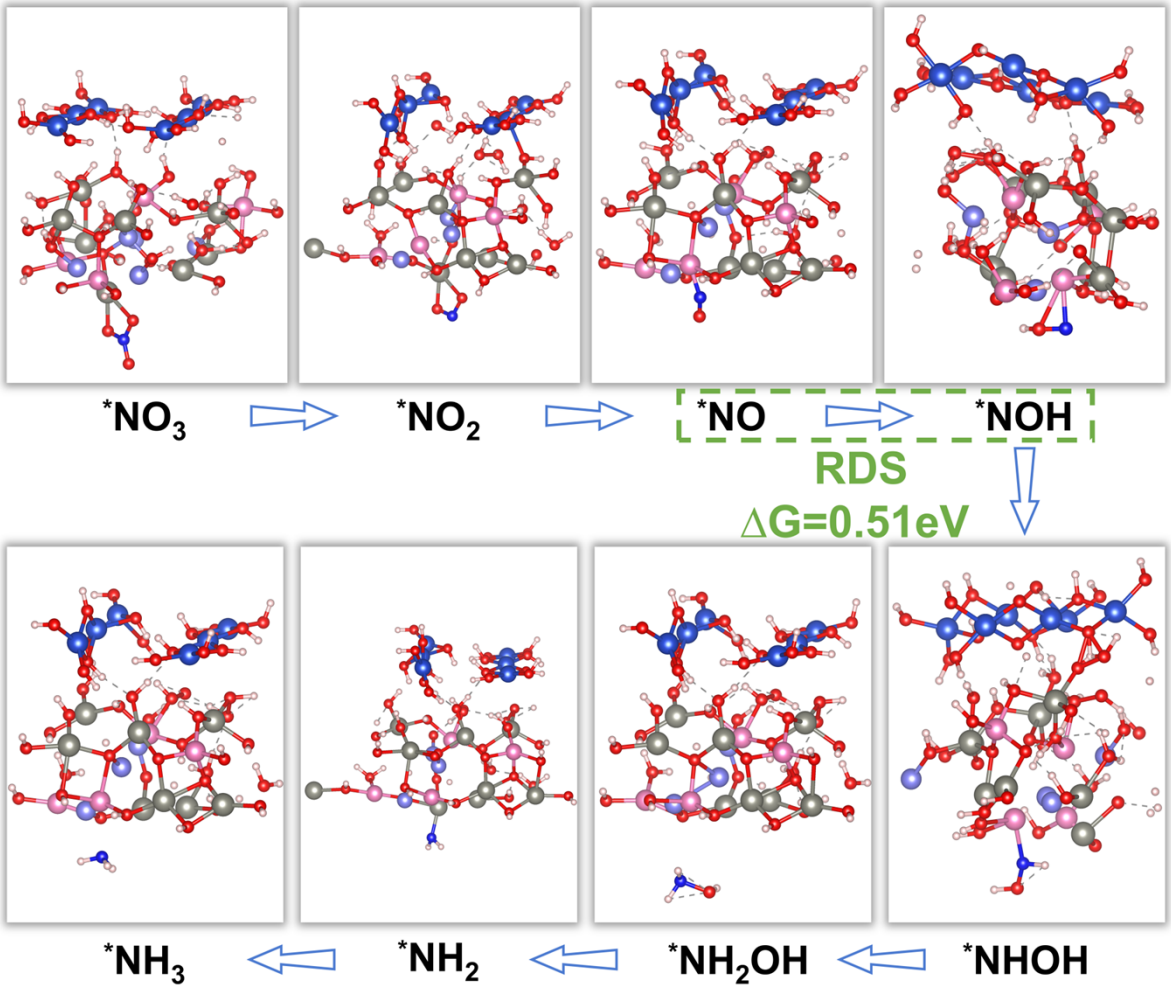


**Fig. S26.** Model diagram of the adsorption of intermediates by Si-ZnCo-LDH/Cu catalyst in the $NO_3^-$RR process.

## 3. Supplementary Tables

**Table. S1.** Ammonia synthetic performances of Si-ZnCo-LDH/Cu at −1.3 V vs. RHE (0.5 M $Na_2SO_4$ containing 0.1 M $NO_3^-$)

| Samples | $NH_3$ Yield rate (mg $h^{-1}$ $cm^{-2}$) | $NH_3$ Faradaic efficiency (%) |
|---|---|---|
| **ZnCo-LDH/Cu** | 16.03 | 58.41 |
| **Si-ZnCo-LDH/Cu-15s** | 17.94 | 65.92 |
| **Si-ZnCo-LDH/Cu-30s** | 25.71 | 93.61 |
| **Si-ZnCo-LDH/Cu-45s** | 16.72 | 60.89 |
| **Si-ZnCo-LDH/Cu-60s** | 14.28 | 52.66 |

*Experimental conditions common to all entries, Applied potential: −1.3 V vs. RHE; Electrolysis time: 1 h; Electrolyte: 100 mM $KNO_3$ + 0.5 M $Na_2SO_4$; Catalyst loading area: 1 $cm^2$.

**Table. S2.** Ammonia synthetic performances of Si-ZnCo-LDH/Cu at varied potentials (0.5 M $Na_2SO_4$ containing 0.1 M $NO_3^-$)

| Samples | Potential (V vs. RHE) | $NH_3$ Yield rate (mg $h^{-1}$ $cm^{-2}$) | $NH_3$ Faradaic efficiency (%) |
|---|---|---|---|
| **Si-ZnCo-LDH/Cu** | −1.1 | 17.57 | 63.51 |
| | −1.2 | 17.79 | 65.73 |
| | −1.3 | 25.71 | 93.61 |
| | −1.4 | 22.33 | 85.79 |
| | −1.5 | 18.08 | 74.51 |

*Experimental conditions common to all entries, Electrolysis time: 1 h; Electrolyte: 100 mM $KNO_3$ + 0.5 M $Na_2SO_4$; Catalyst loading area: 1 $cm^2$.

**Table. S3.** Ammonia synthetic performances of Si-ZnCo-LDH/Cu at −1.3 V vs. RHE (0.5 M $Na_2SO_4$ containing 20, 40, 100, 200 mM $NO_3^-$).

| Samples | Electrolyte solution | $NH_3$ Yield rate ($mg\ h^{-1}\ cm^{-2}$) | $NH_3$ Faradaic efficiency (%) |
|---|---|---|---|
| **Si-ZnCo-LDH/Cu** | 20 mM $KNO_3$ 0.5 M $Na_2SO_4$ | 7.5 | 49.44 |
| | 40 mM $KNO_3$ 0.5 M $Na_2SO_4$ | 14.47 | 73.13 |
| | 100 mM $KNO_3$ 0.5 M $Na_2SO_4$ | 25.71 | 93.61 |
| | 200 mM $KNO_3$ 0.5 M $Na_2SO_4$ | 26.17 | 90.63 |

*Experimental conditions common to all entries, Applied potential: −1.3 V vs. RHE; Electrolysis time: 1 h; Catalyst loading area: 1 $cm^2$.

**Table. S4.** Reported catalysts for the nitrate reduction to ammonia.

| Catalysts | Electrolyte solution | $NH_3$ Yield | $NH_3$ Faradaic efficiency | Zn-$NO_3^-$ Battery | Reference |
|---|---|---|---|---|---|
| **Si-ZnCo-LDH/Cu** | **100 mM $NO_3^-$ 0.5 M $Na_2SO_4$** | **25.71 mg $h^{-1}$ $cm^{-2}$ (−1.3 V vs. RHE)** | **93.61 %** | ○ | **This work** |
| Fe-doped $Co_3O_4$ nanoarray | 50 mM $NO_3^-$ 0.1 M PBS | 0.624 mg $mg_{cat}^{-1}h^{-1}$ (−0.85 V vs. RHE) | 95.5 % | ○ | [1] |
| $Fe_2TiO_5$ nanofiber | 100 mM $NO_3^-$ PBS solution | 0.73 mmol $mg_{cat}^{-1}h^{-1}$ (−1.0 V vs. RHE) | 87.6 % | ○ | [2] |
| $Fe_1$/NC-900 | 500 mM $NO_3^-$ 0.1 M $K_2SO_4$ | ~6 mg $mg_{cat}^{-1}$ $h^{-1}$ (−0.7 V vs. RHE) | 86.7 % | N/A | [3] |
| Np-Cu/$MnO_x$ | 100 mM $NO_3^-$ 0.1 M $K_2SO_4$ | 29.3 mg $mg_{cat}^{-1}$ $h^{-1}$ (−0.6 V vs. RHE) | 86.2 % | N/A | [4] |
| CuCoAl LDH | 50 mM $NO_3^-$ 0.5 M PBS | 0.22 mol $g_{cat}^{-1}$ $h^{-1}$ (0 V vs. RHE) | 99.5 % | N/A | [5] |
| PA-RhCu cNCs | 0.05 M $NO_3^-$ 0.1 M $HClO_4$ | 2.40 mg $h^{-1}$ $mg_{cat}^{-1}$ (−0.05 V vs. RHE) | 93.7 % | N/A | [6] |
| CuO NWAS | 200 ppm $NO_3^-$ 0.5 M $Na_2SO_4$ | 0.2449 mmol $h^{-1}cm^{-2}$ (−0.6 V vs. RHE) | 95.8 % | N/A | [7] |
| $Cu_3Pd_1$ | 50 ppm $NO_3^-$ 0.5 M $K_2SO_4$ | 784.37 $mg^{-1}$ $mg_{cat}^{-1}$ (−0.46 V vs. RHE) | 90.02 % | N/A | [8] |
| Rh@Cu | 100 mM $NO_3^-$ 0.1 M $K_2SO_4$ | 1.27 mmol $h^{-1}$ $cm^{-2}$ (−0.2 V vs. RHE) | 93 % | N/A | [9] |
| BCN@Ni | 100 mM $NO_3^-$ 0.1 M KOH | 2.32 μg $cm^{-2}$ $h^{-1}$ (−0.5 V vs. RHE) | 91.15 % | N/A | [10] |
| Fe/Cu-NG | 100 mM $NO_3^-$ 1 M KOH | 1.08 mmol $mg_{cat}^{-1}h^{-1}$ (−0.5 V vs. RHE) | 92.51 % | N/A | [11] |
| Fe-cyano NSs | 100 mM $NO_3^-$ 1 M KOH | 42.1 mg $mg_{cat}^{-1}$ $h^{-1}$ (−0.5V vs. RHE) | 90 % | N/A | [12] |
| CoP Nas/CFC | 1000 mM $NO_3^-$ 1 M KOH | 9.56 mol $m^{-2}$ $h^{-1}$ (−0.3 V vs. RHE) | ~100 % | N/A | [13] |
| Cu-N-C SAC | 100 mM $NO_3^-$ 0.1 M KOH | 4.5 mg $cm^{-2}$ $h^{-1}$ (−1.0 V vs. RHE) | 84.7 % | N/A | [14] |
| Fe/CoP NHs | 100 mM $NO_3^-$ 1 M KOH | 27.6 mg $mg_{cat}^{-1}$ $h^{-1}$ (−0.25 V vs. RHE) | 93.3 % | N/A | [15] |
| NiCo LDH/Cu NW | 2000 ppm $NO_3^-$ 1 M KOH | 2.35 mmol $cm^{-2}$ $h^{-1}$ (−0.214 V vs. RHE) | 94.25 % | N/A | [16] |
| CuNi-LDHs | 100 mM $NO_3^-$ 0.1 M KOH | 2.73 mg $cm^{-2}$ $h^{-1}$ (−0.4 V vs. RHE) | 94.65 % | N/A | [17] |

**Notes:** "○" and "N/A" denote "existence and non-existence".

**Table. S5.** The Zn-$NO_3^-$ batteries performance comparison of electrode.

| Catalysts | Electrolyte solution | OCV (V vs. $Zn/Zn^{2+}$) | Power density (mW $cm^{-2}$) | Stability (h) | Reference |
|---|---|---|---|---|---|
| **Si-ZnCo-LDH/Cu** | **100 mM $NO_3^-$ 0.5 M $Na_2SO_4$** | **1.432** | **17** | **60 (10 mA $cm^{-2}$)** | **This work** |
| Fe-doped $Co_3O_4$ nanoarray | 50 mM $NO_3^-$ 0.1 M PBS | 1.0 | 0.75 | N/A | [1] |
| $Fe_2TiO_5$ nanofiber | 100 mM $NO_3^-$ PBS solution | 1.5 | 5.6 | 12 | [2] |
| CuTABQ | 50 mM $NO_3^-$ 0.2 M $K_2SO_4$ | N/A | 12.3 | 17 (10 mA $cm^{-2}$) | [18] |
| CoCu-$Ti_3C_2T_x$ | 100 mM $NO_3^-$ 0.1 M $K_2SO_4$ | 1.63 | 10.33 | 24 | [19] |
| Bi-$CoS_2$ | 100 mM $NO_3^-$ 1 M KOH | 1.38 | 16.3 | 12 (15 mA $cm^{-2}$) | [20] |
| CuPd/CuO@NF | 100 ppm $NO_3^-$ 1 M KOH | 1.04 | 53.7 | 24 (20 mA $cm^{-2}$) | [21] |
| $Cu_1$/ZnO | 100 mM $NO_3^-$ 1 M KOH | 1.512 | 5.5 | 12 (1 mA $cm^{-2}$) | [22] |
| HE-OH | 100 mM $NO_3^-$ 1 M KOH | 1.376 | 3.62 | 10 (5 mA $cm^{-2}$) | [23] |
| Cu-RD | 500 ppm $NO_3^-$ 0.11 M KOH | 0.93 | 14.09 | N/A | [24] |
| 0.6W-O-CoP@NF | 100 mM $NO_3^-$ 1 M KOH | 0.7 | 9.27 | N/A | [25] |
| CuCo-TPA-E | 100 mM $NO_3^-$ 1 M KOH | 1.32 | 8.46 | N/A | [26] |

## 4. References


1. P. Wei, J. Liang, Q. Liu, L. Xie, X. Tong, Y. Ren, T. Li, Y. Luo, N. Li, B. Tang, A. M. Asiri, M. S. Hamdy, Q. Kong, Z. Wang and X. Sun, *J. Colloid Interface Sci.*, 2022, **615**, 636-642.
2. H. Du, H. Guo, K. Wang, X. Du, B. A. Beshiwork, S. Sun, Y. Luo, Q. Liu, T. Li and X. Sun, *Angew. Chem. Int. Ed.*, 2022, **135**, e202215782.
3. L. Liu, T. Xiao, H. Fu, Z. Chen, X. Qu and S. Zheng, *Appl. Catal. B Environ.*, 2023, **323**, 122181.
4. Y. Cui, A. Dong, Y. Zhou, Y. Qu, M. Zhao, Z. Wang and Q. Jiang, *Small*, 2023, **19**, 2207661.
5. W. Wang, J. Chen and E. C. M. Tse, *J. Am. Chem. Soc.*, 2023, **145**, 26678-26687.
6. Z. X. Ge, T. J. Wang, Y. Ding, S. B. Yin, F. M. Li, P. Chen and Y. Chen, *Adv. Energy Mater.*, 2022, **12**, 2103916.
7. J. Qin, L. Chen, K. Wu, X. Wang, Q. Zhao, L. Li, B. Liu and Z. Ye, *ACS Appl. Energy Mater.*, 2021, **5**, 71-76.
8. Y. Xu, K. Ren, T. Ren, M. Wang, M. Liu, Z. Wang, X. Li, L. Wang and H. Wang, *Chem. Commun.*, 2021, **57**, 7525-7528.
9. H. Liu, X. Lang, C. Zhu, J. Timoshenko, M. Rüscher, L. Bai, N. Guijarro, H. Yin, Y. Peng, J. Li, Z. Liu, W. Wang, B. R. Cuenya and J. Luo, *Angew. Chem. Int. Ed.*, 2022, **61**, e202202556
10. X. Zhao, Z. Zhu, Y. He, H. Zhang, X. Zhou, W. Hu, M. Li, S. Zhang, Y. Dong, X. Hu, A. V. Kuklin, G. V. Baryshnikov, H. Ågren, T. Wågberg and G. Hu, *Chem. Eng. J.*, 2022, **433**, 133190
11. S. Zhang, J. Wu, M. Zheng, X. Jin, Z. Shen, Z. Li, Y. Wang, Q. Wang, X. Wang, H. Wei, J. Zhang, P. Wang, S. Zhang, L. Yu, L. Dong, Q. Zhu, H. Zhang and J. Lu, *Nat. Commun.*, 2023, **14**, 3634.
12. Z. Fang, Z. Jin, S. Tang, P. Li, P. Wu and G. Yu, *ACS Nano*, 2021, **16**, 1072-1081.
13. S. Ye, Z. Chen, G. Zhang, W. Chen, C. Peng, X. Yang, L. Zheng, Y. Li, X. Ren, H. Cao, D. Xue, J. Qiu, Q. Zhang and J. Liu, *Energy & Environmental Science*, 2022, **15**, 760-770.
14. J. Yang, H. Qi, A. Li, X. Liu, X. Yang, S. Zhang, Q. Zhao, Q. Jiang, Y. Su, L. Zhang, J.-F. Li, Z.-Q. Tian, W. Liu, A. Wang and T. Zhang, *J. Am. Chem. Soc.*, 2022, **144**, 12062-12071.
15. Q.-L. Hong, Z.-N. Zhang, X.-H. Wang, S.-B. Yin, F. Shi, S.-N. Li and Y. Chen, *Inorg. Chem.*, 2022, **61**, 14397-14402.
16. X. Zhang, X. Liu, Z.-F. Huang, L. Guo, L. Gan, S. Zhang, M. Ajmal, L. Pan, C. Shi, X. Zhang, G. Yang and J.-J. Zou, *ACS Catal.*, 2023, **13**, 14670-14679.
17. H. Li, S. Li, R. Guan, Z. Jin, D. Xiao, Y. Guo and P. Li, *ACS Catal.*, 2024, **14**, 12042-12050.
18. R. Zhang, H. Hong, X. Liu, S. Zhang, C. Li, H. Cui, Y. Wang, J. Liu, Y. Hou, P. Li, Z. Huang, Y. Guo and C. Zhi, *Angew. Chem. Int. Ed.*, 2023, **62**, e202309930.

19. Z. Cui, P. Zhao, H. Wang, C. Li, W. Peng and J. Liu, *Adv. Funct. Mater.*, 2024, **34**, 2410941.
20. C. M. Yang, T. T. Wei, C. T. Wang, F. Yue, X. Li, H. J. Pang, X. Y. Zheng, Y. T. Zhang and F. Fu, *Mater. Horiz.*, 2025, **12**, 877-885.
21. J. Li, L. Liu, S. Huang, H. Wang, Y. Tang, C. Zhang, F. Du, R. Ma, C. Li and C. Guo, *Adv. Funct. Mater.*, 2025, DOI: 10.1002/adfm.202501527, 2501527.
22. Z. Chen, Y. Zhao, H. Huang, G. Liu, H. Zhang, Y. Yan, H. Li, L. Liu, M. Liu, D. Wang and J. Zeng, *J. Am. Chem. Soc.*, 2025, **147**, 18737-18746.
23. M. Chen, X. Li, N. Liu, Z. Du, Z. Wang and J. Qi, *Chin. Chem. Lett.*, 2025, **36**, 111294.
24. H. Jiang, G. F. Chen, O. Savateev, J. Xue, L. X. Ding, Z. Liang, M. Antonietti and H. Wang, *Angew. Chem. Int. Ed.*, 2023, **135**, e202218717.
25. Z. Chang, G. Meng, Y. Chen, C. Chen, S. Han, P. Wu, L. Zhu, H. Tian, F. Kong, M. Wang, X. Cui and J. Shi, *Adv. Mater.*, 2023, **35**, 2304508.
26. J. Yang, W.-D. Zhang, H. Zhao, Y. Zou, Z.-Y. Zhang, J. Liu, J. Wang, Z.-G. Gu and X. Yan, *Appl. Catal. B Environ.*, 2024, **340**, 123237.